# 2D axial-symmetric model for fluid flow and heat transfer in the melting and resolidification of a vertical cylinder

S. MORVILLE[1], M. CARIN[1], M. MULLER[2], M. GHARBI[2], P. PEYRE[2], D. CARRON[1], P. LE MASSON[1], R. FABBRO[2]
[1] Laboratoire LIMATB, Université de Bretagne Sud, Rue Saint Maudé, 56321 Lorient Cedex, FRANCE
[2] Laboratoire PIMM, UMR 8006, CNRS-Arts et Métiers ParisTech, 151, boulevard de l'Hôpital – 75013 Paris, FRANCE
*Corresponding author: simon.morville@univ-ubs.fr

**Abstract:** Direct Metal Laser Deposition (DMLD) is a process, different from molding or machining, which allows the producing of fully densified and operational components. This technique involves injecting metal powder through a coaxial nozzle into a melt pool obtained by a moving laser beam. The final object is obtained by superimposing the layers created by the process. The roughness of the functional part is strongly conditioned by surface tension and its temperature dependence, which is called Marangoni effect. In order to study this process, we have first developed a simple model to predict the geometry after resolidification of the molten zone of a rod heated at its top with a laser source. The energy and momentum equations are solved in a two-dimensional axial-symmetric reference. The deformation of free surface is calculated using a moving mesh by the way of the ALE method. The calculated temperatures are compared with thermocouple measurements. The calculated dynamic shape of the free surface during melting and resolidification is compared with data obtained from high speed videos. Macrographs are also used to validate the position of the solid/liquid interface.

**Keywords:** free surface, surface tension, Marangoni, ALE, heat transfer, fluid flow, phase-change, laser.

## 1. Introduction

Direct Metal Laser Deposition (DMLD) is a very promising technique for the rapid manufacturing, part repairing, or surface treatment of metals. This technique involves injecting metal powder through a nozzle into a melt pool obtained by a moving laser beam. The final object is obtained by superimposing the layers created by the process. Although the advantages of the process are widely recognized, one of the greatest current limitations of DMLD process comes from deleterious surface finish, as illustrated in Figure 1.

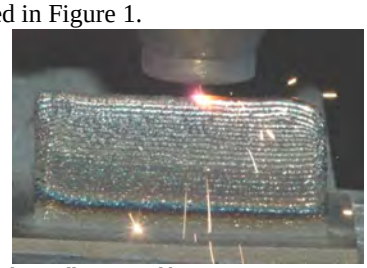

**Figure 1:** Thin wall generated by DMLD

To limit the roughness defaults, numerical modeling offers an efficient way to better understand the complicated physics responsible for the surface finish. The DMLD process involves complex physical phenomena, such as laser-powder interactions, heat transfer, melting, fluid flow, solidification and possible evaporation. In the past decade, many analytical and numerical models have been developed to simulate the laser direct metal deposition process. Labudovic et al. [1] have developed a three-dimensional model of heat transfer and residual stresses for direct metal laser deposition process using both numerical and analytical approaches. In their model, the element birthing method was employed to simulate the formation of layer but its shape was assumed to be known. Several authors have proposed analytical or numerical models to determine multiple-layer clad geometry based on energy and mass balances [2][3]. In these works, the effects of Marangoni phenomena and hydrodynamic of the liquid metal are taken into account through an enhanced thermal conductivity. Toyserkani [2] takes into account the laser power attenuation and Brewster effects to include the changes in absorption factor due to the clad geometry. Peyre et al. [4] have used Comsol Multiphysics software to predict multiple-layer clad geometry combining analytical and numerical models. They used a specific function for thermal conductivity to simulate the generation of up to

20 layers due to powder deposition and validate their numerical results with thermocouples and high speed camera comparisons for TA6V titanium alloy. However most of those models have neglected the fluid flow in the melt pool. The shape of the clad was predicted using mass conservation only and ignoring the surface tension effect.

The most sophisticated models take into account heat transfer, phase changes, mass addition, fluid flow, interactions between the laser beam and the powder flow. To track the liquid/gas interface and simulate the continuous addition of material, some authors used the level-set method [5] or the Volume-Of-Fluid method [6]. Two forces are considered at the liquid/gas interface: the capillary, which acts in the normal direction due to interface curvature and surface tension, and thermocapillary forces acting in the tangential direction of the liquid free surface (Marangoni effect).

In this work, we have chosen the Arbitrary-Lagrangian Eulerian (ALE) method to track the liquid/gas interface. This method has the advantage to maintain the interface discontinuity and explicitly tracks its evolution. To validate our model, we have studied a very simplified case which consists in predicting the geometry after resolidification of the molten zone of a rod heated at its top with a laser source. The work presented here constitutes a preliminary study for the direct metal laser deposition, but it includes most of the physical phenomena except for material addition and laser/powder interaction. This 2D axial-symmetric transient model takes into account heat transfer, phase changes and fluid flow. The calculated temperatures are compared with thermocouples measurements. The calculated dynamic shape of the free surface during melting and resolidification is compared with data obtained from high speed videos. Macrographs are also used to validate the extreme position of the solid/liquid interface. This study based on a simple configuration aims to validate the input values of the model, such as material properties, especially those of the liquid metal which are difficult to measure.

The experimental set-up is briefly described in section 2. The physical model and associated assumptions used in this study are presented in section 3. Mathematical formulations and boundary conditions of each physical model are given thereafter. The numerical and experimental results are compared in section 4.

## 2. Experimental setup

In this study, a TRUMPF TruDisk 10002 disk laser (λ=1.03μm) is used to irradiate the top of a metallic rod of 3.2 mm diameter and 30 mm length (Figure 2a). This vertical cylinder is hold in a 3-point chuck. The laser beam radius is 3.14 mm with spatially-homogeneous energy distribution. The upper extremity of the rod is introduced into a transparent pipe of 16 mm internal diameter to ensure shielding of the melt pool with argon flow.

A Photron Ultima 1024 high speed camera with a recording rate of 1 kHz is used to monitor liquid/gas interface evolution in a normal plane to the sample. The camera is coupled with a KG3 filter to enhance picture quality.

The surface temperatures are measured by four thermocouples (type K) welded along the lateral surface of the sample, as shown in Figure 2b.

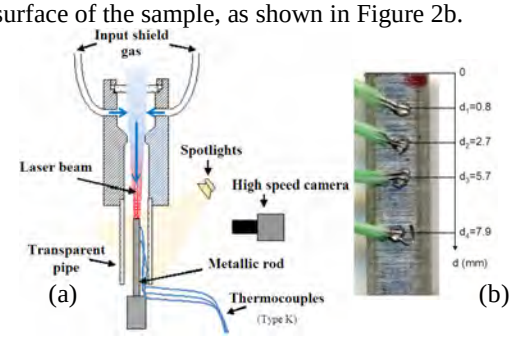


**Figure 2: (a)** Experimental setup device of the melting of a rod with shield gas; **(b)** positioning of thermocouples

## 3. 2D axial-symmetric model

Under the irradiation of the laser beam, the metallic rod reaches melting temperature and a melt pool grows at the top surface. When the melt pool width is equal to the diameter of the sample, the liquid surface is then deformed due to surface tension and a drop appears at the top of the rod (Figure 3). The volume of the drop will depend on the heating duration. When the laser beam is shut down, the drop solidifies and the sample is naturally cooled to room temperature. The irradiation time is chosen to avoid the collapse of the melting pool along the lateral surface of the rod. The final shape of the rod extremity is strongly dependent on the dynamic evolution of the free surface during

melting. Large gradients of temperature and surface tension exist at the surface of the melt pool, which are also the driving forces for fluid flow. The temperature gradients generate natural convection, as well known as Buoyancy effect or gravitational convection. At the liquid/gas interface, tension surface gradients introduce a tangential displacement of the liquid metal (Marangoni effect). Fluid flow direction directly depends on chemical surfactant components rate and temperature level.

To predict the evolution of the liquid/gas interface during heating and solidification, a mathematical model has been developed, based on the following assumptions:

- The laser beam intensity profile is assumed to be homogeneous along the R and Z directions (Top Hat distribution); the depth-of-focus effect is ignored.
- The liquid metal is assumed to be an incompressible Newtonian fluid. Flow in the molten pool is considered to be laminar.
- Buoyancy force and gravity are neglected. A parametric study has shown that their effects on final shape are not significant (see Section 4).
- Huge difference of viscosity and density between liquid metal and air allows us to reduce domain computation without considering the air.

### 3.1 Mathematical model

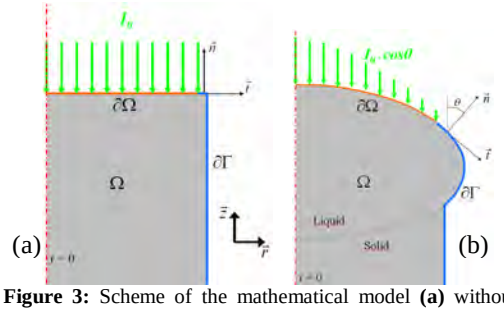


**Figure 3:** Scheme of the mathematical model **(a)** without liquid phase; **(b)** with liquid phase

The transient temperature distribution T(r,z,t) is obtained from the heat conduction equation solved in the metallic rod:

$$\rho c_p\left[\frac{\partial T}{\partial t}+\vec{\nabla}.(\vec{u}T)\right]-\vec{\nabla}\cdot(\lambda\vec{\nabla}T)=0 \qquad (1)$$

where λ is thermal conductivity ($W.m^{-1}.K^{-1}$), $c_p$ is specific heat capacity ($J.kg^{-1}.K^{-1}$), ρ is density ($kg.m^{-3}$), t is time (s), $\vec{u}$ is velocity field in the melt pool ($m.s^{-1}$). This velocity field is calculated from momentum conservation equations, which can be expressed as follows:

$$\rho\left(\frac{\partial\vec{u}}{\partial t}+(\vec{u}-\vec{u}_m).(\nabla\vec{u})\right)=\vec{\nabla}.\left(-pI+\mu\left(\vec{\nabla}\vec{u}+(\vec{\nabla}\vec{u})^T\right)\right)+\vec{S}_u \qquad (2a)$$

$$\vec{\nabla}\cdot\vec{u}=0 \qquad (2b)$$

with

$$\vec{S}_u=-C\frac{(1-f_L)^2}{(f_L{}^3+b)}\vec{u} \qquad (3)$$

where $\vec{u}_m$ is mesh velocity (ALE mode), p is pressure in the fluid (Pa), μ is dynamic viscosity (Pa.s). $\vec{S}_u$ is the frictional dissipation in the mushy zone according to the Carman-Kozeny approximation derived from Darcy's law [7]. C is a constant parameter depending on morphology and size of the dendrites. In the present study, the value of C is set to $10^{12}$. b is a constant equal to 0.001 to avoid division by zero. The effect of latent heat of fusion on the temperature distribution can be approximated by increasing the specific heat capacity as:

$$c_p{}^*=L_f.\frac{df_L}{dt}+c_p \qquad (4)$$

where $c_p$* is modified heat capacity ($J.kg^{-1}.K^{-1}$), $L_f$ is the latent heat of fusion ($J.kg^{-1}$), $f_L$ is the liquid fraction, which is expressed as:

$$f_L=\begin{cases}0 & T_S\le T\\ \dfrac{T-T_S}{T_L-T_S} & T_S<T<T_L\\ 1 & T<T_L\end{cases} \qquad (5)$$

$T_S$ and $T_L$ are respectively the solidus and liquidus temperatures for the considered alloy. The boundary conditions for the energy problem and momentum problem are listed below:

a- Energy problem:

$$q|_{\partial\Omega}=\begin{cases}\alpha(\theta).I_0(r,t)-h_c(T-T_0)-\varepsilon\sigma\left(T^4-T_0^4\right) & if\ \partial\Omega\in\partial\Gamma\\ -h_c(T-T_0)-\varepsilon\sigma\left(T^4-T_0^4\right) & if\ \partial\Omega\notin\partial\Gamma\end{cases} \qquad (6)$$

where $I_0(r,t)$ is the laser energy distribution on the metallic rod ($W.m^{-2}$), α is the absorption factor, $h_c$ is the heat convection coefficient ($W.m^{-2}.K^{-1}$), ε is emissivity, σ is Stefan-Boltzmann constant ($5.67.10^{-8}$ $W.m^{-2}.K^{-4}$), ∂Γ is the metallic rod surface ($m^2$), ∂Ω is the surface area irradiated by the laser beam ($m^2$) and $T_0$ is the reference temperature (K).

A continuum laser beam with homogeneous intensity is considered for the energy distribution. The laser beam intensity profile $I_0$ ($W.m^{-2}$) is:

$$I_0(r,t)=\begin{cases}\frac{P_l}{\pi.r_l^2}\delta(t) & if\ \ r\le r_l\\ 0 & if\ \ r>r_l\end{cases} \qquad (7)$$

where $P_l$ is the incident laser power (W), $r_l$ is laser beam radius, $\delta = 1$ when the laser is turned on and $\delta = 0$ when it is turned off.

Due to the deformation of liquid/gas interface, a coefficient depending on angle between laser source and free surface is introduced in the effective energy distribution on free boundary. It acts as a modified absorptivity [8] as:

$$\alpha(\theta)=\alpha_0.\cos(\theta) \qquad (8)$$

where $\alpha_0$ is the absorptivity of a flat surface normally irradiated, $\theta$ is angle between surface normal and laser beam incidence. Adequate values of $\alpha_0$ have been obtained from comparison between numerical and experimental thermal kinetics.

This assumption on absorptivity neglects Brewster effect which postulates that light with specific polarisation reaches a maximum absorptivity at a specific incidence angle.

The other boundary conditions are a zero flux on the symmetry axis and convective and radiative losses at the bottom.

b- Momentum problem:

On the free surface, capillary and thermocapillary forces act both on the normal direction and on the tangential direction. The corresponding equations are:

- in the normal direction:

$$\sigma\,\vec{n}=-P_a\,\vec{n}+\kappa\,\gamma\,\vec{n} \qquad (9a)$$

- in the tangential direction:

$$\sigma_t=\frac{\partial\gamma}{\partial T}\vec{\nabla}T\cdot\vec{t} \qquad (9b)$$

where $P_a$ is the ambient pressure (Pa), $\kappa$ is the curvature ($m^{-1}$) and $\gamma$ is the surface tension coefficient ($N.m^{-1}$). $\vec{n}$ and $\vec{t}$ are respectively the normal and tangential vectors to the free surface.

These boundary conditions are manually implemented as a weak constraint on free surfaces. The details of the implementation for the capillary forces can be found in [9].

Axial symmetry condition is applied for r = 0. Other boundaries are defined as open boundaries.

3-2 Moving mesh

The computational domain includes two moving interfaces: a liquid/solid interface and a liquid/gas interface. Only the liquid/gas interface is explicitly tracked using an ALE method. In this method, the displacement of boundary nodes is controlled by the fluid mechanics phenomena and is insured by a Lagrangian description whereas domain nodes follow an almost Eulerian description. Internal nodes are nevertheless moved to avoid numerical instabilities when computing. Comsol Multiphysics® proposes two smoothing algorithms to control the displacement of the nodes: Winslow and Laplace. The calculations presented in this paper are performed using Winslow method.

Coupling of ALE method with momentum conservation equations is made through expression (10):

$$V_{mesh}.\vec{n}=V_{mat}.\vec{n} \qquad (10)$$

with $V_{mesh}$ the mesh velocity ($m.s^{-1}$) and $V_{mat}$ the material velocity ($m.s^{-1}$) computed from momentum conservation equations.

3-3 Thermophysical properties

The material used in this study is a high mechanical performance steel (S355 steel). Thermal conductivity, density and specific heat capacity are temperature dependant and taken from OTUA [10].

In the absence of available data for S355 steel, the capillary and thermocapillary coefficients of stainless steel are used [11]. These coefficients depend on temperature and sulphur content, as follows:

$$\gamma\left(mN.m^{-1}\right)=1840-0.4\,(T-T_M)-0.056.T.\ln(B) \qquad (11)$$

$$\frac{\partial\gamma}{\partial T}\left(mN.m^{-1}.K^{-1}\right)=-0.4-0.056\left(\frac{28798\,(1-B)}{B.T}+\ln(B)\right) \qquad (12)$$

with

$$B=1+(0.68.\%S).e^{\left(\frac{28798}{T}-8.5647\right)} \qquad (13)$$

## 4. Results and discussion

The mesh consists of 13554 triangular elements with a maximum size of 10 µm on open boundaries and 50 µm inside the domain. The equations are solved using PARDISO solver. The computation time requires about 660 min on

a computer equipped with a 2 processors Intel Core 2 Duo CPU 2.4 GHz and 3.5 Go RAM.

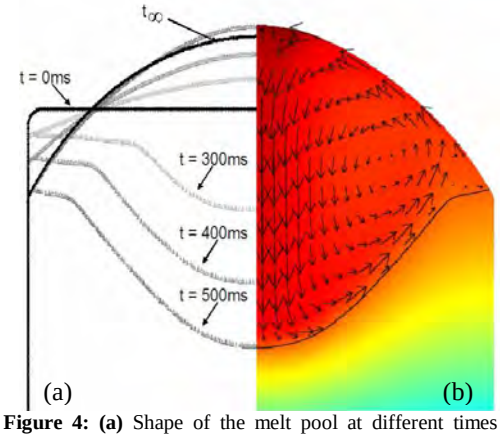


**Figure 4: (a)** Shape of the melt pool at different times – t = 0 ms, 300 ms, 400 ms, 500 ms and fully solidified; **(b)** Velocity and temperature fields at t = 500 ms, maximum amplitude: $V_{max}$ = 0.615 m.s$^{-1}$, $T_{max}$ = 2170 K

The calculations are performed with an incident power of 962 W during 500 ms. Figure 4a presents the evolution of the melt pool shape at different time steps. Capillary forces significantly governed the deformation of the liquid/gas interface by constraining it to keep a drop shape during the growth of the melt pool. Thermocapillary forces are distinctly driving the fluid flow in the melt pool. The levels of temperature, depending on laser power and absorptivity, are such that thermocapillary coefficient is positive. Fluid flow is then directed from the coldest region of the surface towards the warmest region (figure 4b). This induces a fluid motion diving along the symmetry axis, thus leading to a deep melt pool.

Due to the advection in the melt pool, the temperature is relatively homogeneous in the liquid phase whereas the temperature gradients are larger in the solid phase.

Figure 5 shows the good agreement between the calculated and measured temperatures at the rod surface, both during heating and cooling. We can note that the acquisition fails for thermocouple n°1 at around t = 500 ms due to the high temperatures reached.

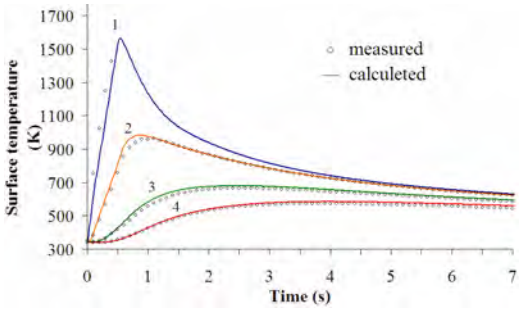


**Figure 5:** Comparison of the surface thermal kinetics between experimental and numerical results at different Z-coordinates given in Figure 2b

Figure 6 compares the calculated and measured melt pool shapes at different times. The dynamic position of the liquid/gas interface is tracked by the high speed camera and is perfectly predicted by the model. After solidification and cooling, macrographs are performed in order to estimate the location of liquid/solid interface (the front fusion propagation is supposed to have been immediately stopped when laser pulse was off). The difference between calculated and measured liquid/solid interfaces is around 27% on the maximum melt pool depth using the following expression $(h_{cal} - h_{mea})/h_{mea}$, where $h_{cal}$ and $h_{mea}$ are defined in Figure 6. This discrepancy results probably from the uncertainty in material properties. However we observe on the macrograph the same phenomenon of digging in the middle of the rod, which confirms that thermocapillary forces are quite well described in the model.

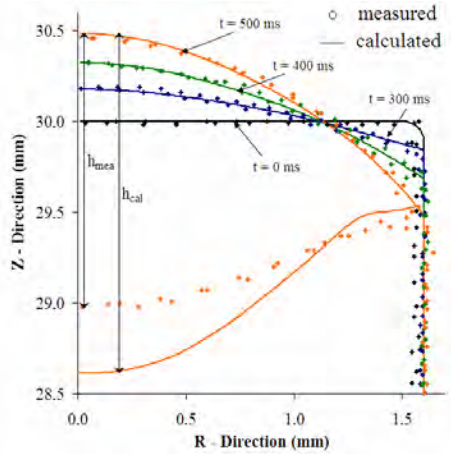


**Figure 6:** Comparison of the shape of the liquid/gas interface between experimental values and numerical results at t = 0, 300, 400 and 500 ms

In order to study the influence of material properties, a parametric study has been performed. To simplify, all parameters are kept constant in the computations but differ for the solid (S) and liquid (L) phases. Reference parameter values are given in Table 1. Each of them is independently increased by 25% to evaluate their sensibility on the melt pool shape. Results show that thermal properties significantly modify the depth of the melt pool. The discrepancy between numerical and experimental can then be explained partially by the inaccuracy of the thermal properties. The increase of thermal conductivity, density or heat capacity induces a reduction of the melt pool size, since it increases the thermal diffusivity or thermal inertia of the material. Absorptivity coefficient influences also significantly the melt pool shape, but as previously mentioned, this parameter was evaluated by comparing numerical and experimental results. The other properties have no significant effect on the melt pool shape.

| | Reference values | Relative error (%) $(h_{cal}-h_{ref})/h_{ref}$ |
|---|---|---|
| Thermal conductivity (S-L) | 40-32 $W.m^{-1}.K^{-1}$ | -13.5 |
| Heat capacity (S-L) | 500-710 $J.kg^{-1}.K^{-1}$ | -23.8 |
| Density (S-L) | 7800-7290 $kg.m^{-3}$ | -22.1 |
| Dynamic viscosity | $5.10^{-3}$ Pa.s | -1.6 |
| Capillary coefficient | 1.5 $N.m^{-1}$ | <1 |
| Thermocapillary coefficient | $10^{-4}$ $N.m^{-1}.K^{-1}$ | 2.1 |
| Absorptivity coefficient | 0.3 | 32.4 |
| Emissivity coefficient | 0.5 | <1 |
| Latent heat of fusion | $2.5.10^{5}$ $J.kg^{-1}$ | 1 |

**Table 1**: Relative melt pool depth error between modified and reference computation

Due to the small perturbation (25%), the thermocapillary coefficient does not appear as a key parameter. Nonetheless, Figure 7 shows that with larger amplitudes and different signs of the thermocapillary coefficient, the melt pool shape is strongly modified. It appears that the constant values specified in Table 1 for capillary and thermocapillary coefficients reduces the discrepancy between experimental and calculated results (relative error on the melt pool depth: 12%). Moreover, these values do not affect the validation of thermal cycles.

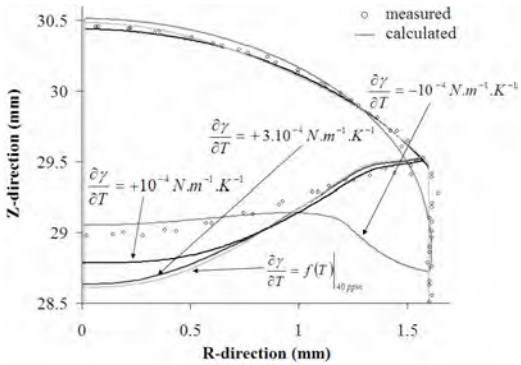


**Figure 7:** Comparison of melt pool shape at t = 500 ms with different thermocapillary coefficients

In order to study the influence of gravity, computations were performed by adding the following term in the equation 2a:

$$\vec{F}_v = \rho_0\left(1-\beta(T-T_0)\right)\vec{g} \qquad (14)$$

where $\rho_0$ represents the density at the reference temperature $T_0$, $\beta$ is the coefficient of thermal expansion and is equal to $10^{-4}$ $K^{-1}$ and $\vec{g}$ is gravity vector.

The error on the maximum melt pool depth is less than 1%, indicating that gravity and buoyancy can then be neglected in our calculations. This conclusion can also be demonstrated by evaluating dimensionless numbers, such as Bond, Rayleigh and Marangoni numbers.

Bond number represents the ratio of gravity forces to surface tension forces:

$$Bo = \frac{\Delta\rho.g.L_c^{\,2}}{\gamma} \qquad (15)$$

with $L_c$ the characteristic length (here the radius of the rod), $\Delta\rho$ is the difference between the liquid density and air density. In our case, the Bond number is Bo = 0.12 and confirms that gravity forces are negligible.

Rayleigh number compares thermocapillary forces with viscous forces:

$$Ra = \frac{g.\beta.\Delta T.L_c^3}{\nu^2}.\mathrm{Pr} \qquad (16)$$

where $\nu$ is kinematic viscosity ($m^2.s^{-1}$) and Pr is Prandtl number.

Marangoni number is the ratio of buoyancy forces and thermal and momentum diffusivities.

$$Mg = \frac{\partial\gamma}{\partial T}.\frac{L_c.\Delta T}{\mu.a} \qquad (17)$$

where a is the thermal diffusivity ($m^2.s^{-1}$).
The ratio of Marangoni and Rayleigh number compares the contribution of thermocapillary effect with natural convection at liquid/gas interface [12]. It leads to Mg/Ra = 5.5 and shows that thermocapillary forces strongly determines velocity field in the liquid metal, and thus melt pool shape. This explains why buoyancy forces are negligible in our calculations.

## Conclusion

This paper presents preliminary results concerning the study of a Direct Metal Laser Deposition process. A 2D axial-symmetry model was developed using Comsol Multiphysics® version 3.5a. The model successfully predicts, with ALE method, the geometry after resolidification of the molten zone of a rod heated at its top by a laser source. Consequently simplifying assumptions and input parameter values were validated. It was shown that the liquid/gas interface shape is mainly governed by surface tension whereas the solid/liquid interface is controlled by Marangoni convection. The gravity and buoyancy forces were found insignificant for the case studied. The parameter study has shown that thermal properties have to be known with accuracy in order to predict correctly the melt pool volume.

Further works will include powder feeding and computing in a 3D framework using ALE method.

## Acknowledgements

The authors would like to acknowledge the financial support by the French National A.N.R in the frame of the project “ASPECT” referenced by AMR-09-BLAN-0014-02.

## References

[1] M. Labudovic, D. Hu, R. Kovacevic, “A three dimensional model for direct laser metal powder deposition and rapid prototyping,” *Journal of Materials Science*, vol. 38, Jan. 2003, p. 35-49.

[2] E. Toyserkani, A. Khajepour, S. Corbin, “3-D finite element modeling of laser cladding by powder injection: effects of laser pulse shaping on the process,” *Optics and Lasers in Engineering*, vol. 41, Juin. 2004, p. 849-867.

[3] A.J. Pinkerton, L. Li, “Modelling the geometry of a moving laser melt pool and deposition track via energy and mass balances,” *Journal of Physics D: Applied Physics*, vol. 37, 2004, p. 1885-1895.

[4] P. Peyre, P. Aubry, R. Fabbro, R. Neveu, A. Longuet, “Analytical and numerical modelling of the direct metal deposition laser process,” *Journal of Physics D: Applied Physics*, vol. 41, 2008, p. 025403.

[5] L. Han, K. Phatak, F. Liou, “Modeling of laser cladding with powder injection,” *Metallurgical and Materials Transactions B*, vol. 35, Déc. 2004, p. 1139-1150.

[6] F. Liou, Z. Fan, H. Pan, J. Newkirk, K. Slattery, H. Chou, M. Kinsella, *Modeling and Simulation of a Laser Deposition Process (Preprint)*, 2007.

[7] A.D. Brent, V.R. Voller, K.J. Reid, “Enthalpy–Porosity Technique for Modeling Convection–Diffusion Phase Change: Application to the Melting of a Pure Metal,” *Numerical Heat Transfer, Part B: Fundamentals: An International Journal of Computation and Methodology*, vol. 13, 1988, p. 297-318.

[8] M. Picasso, A. Hoadley, “Finite element simulation of laser surface treatments including convection in the melt pool,” *International Journal of Numerical Methods for Heat & Fluid Flow*, vol. 4, 1994, p. 61-83.

[9] M. Carin, “Square drop oscillation under surface tension - 2D axi-symmetric model”, www.comsol.fr/community/exchange/ (2009).

[10] Données physiques sur quelques aciers d’utilisation courante. Code 15004, Edition OTUA (www.otua.org/Prop_Physiques/FicheOTUA/OTUA2.html).

[11] Y. Su, Z. Li, K.C. Mills, “Equation to estimate the surface tensions of stainless steels,” *Journal of Materials Science*, vol. 40, 2005, p. 2201-2205.

[12] A. M. Bianchi, Y. Fautrelle, J. Etay, *Transferts thermiques*. PPUR presses polytechniques, 2004.